Late Cretaceous seasonal ocean variability from the Arctic.

Andrew Davies[1‡], Alan E. S. Kemp[1]*, Jennifer Pike[2]

[1] National Oceanography Centre Southampton, School of Ocean and Earth Science, University of Southampton, Southampton, SO14 3ZH, UK.

[2] School of Earth and Ocean Sciences, Cardiff University, Main Building, Park Place, Cardiff, CF10 3YE, UK.

*To whom correspondence should be addressed, E-mail: aesk@noc.soton.ac.uk

‡ Present address: Neftex Petroleum Consultants Ltd, 97 Milton Park, Abingdon, OX14 4RY, UK.

Abstract

The modern Arctic Ocean is regarded as barometer of global change and amplifier of global warming[1] and therefore records of past Arctic change are of a premium for palaeoclimate reconstruction. Little is known of the state of the Arctic Ocean in the greenhouse period of the late Cretaceous, yet records from such times may yield important clues to its future behaviour given current global warming trends. Here we present the first seasonally resolved sedimentary record from the Cretaceous from the Alpha Ridge of the Arctic Ocean. This "paleo-sediment trap" provides new insights into the workings of the Cretaceous marine biological carbon pump. Seasonal primary production was dominated by diatom algae but was not related to upwelling as previously hypothesised[2]. Rather, production occurred within a stratified water column, involving specially adapted species in blooms resembling those of the modern North Pacific Subtropical Gyre[3], or those indicated for the Mediterranean sapropels[4]. With elevated CO_2 levels and warming currently driving increased stratification in the global ocean[5] this stratified-adapted style of production may become more widespread. Our evidence for seasonal diatom production and flux testify to an ice free summer, but thin accumulations of terrigenous sediment within the diatom ooze are consistent with the presence of intermittent sea ice in the winter, supporting a wide body of evidence for low Arctic late Cretaceous winter temperatures[6-8] rather than recent suggestions of a 15°C mean annual temperature at this time[9].

The Arctic is a critical yet under-sampled region for palaeoclimate studies. The recent ACEX coring has provided Arctic records back to the Palaeogene[10] but earlier shallow coring of older, Cretaceous sediments has hitherto offered only tantalising indications of the Arctic palaeoenvironment [2, 9, 11, 12]. Such sediments afford the opportunity to investigate Arctic climate variability in past greenhouse states that may be analogues for the future. Specifically, little is known of Arctic seasonal-scale climate variability in periods without permanent sea ice cover. Cretaceous laminated sediments also provide a "palaeo-sediment trap" record whereby the past workings of the marine biological carbon pump may be elucidated. In the modern ocean diatom algae are responsible for up to 40% of oceanic primary production and because they dominate export in many marine environments, diatoms are the key agents in the marine biological carbon pump, central to biogeochemical cycling[13, 14]. By contrast, the role of diatoms in the Cretaceous oceans is poorly understood, in part, due to lack of preservation, since opal A is unstable and diatoms are easily destroyed during sediment burial and silica diagenesis. However, the first, albeit rare, pelagic diatomites occur in the late Cretaceous coinciding with a radiation of planktonic diatoms[15], and in late Cretaceous sediments without surviving biosilica, there is increasing biomarker evidence of diatom contribution to carbon cycling, including the production that generated the black shale horizons of this period[16].

With remarkable serendipity, successive US and Canadian expeditions that occupied floating ice islands above the Alpha Ridge of the Arctic ocean, recovered cores containing shallow buried upper Cretaceous diatom ooze with superbly preserved diatoms (cores Fl-437 and CESAR-6 respectively; taken some 160 km apart) (Figs. 1, 2)[2, 11]. A third core (Fl-533) contains organic carbon-rich mud with no biosilica but with biomarker evidence for the presence of rhizosolenid diatoms[9]. Detailed diatom micropalaeontology of the material we analysed from the CESAR-6 core shows no evidence for evolutionary biostratigraphic change

and diatom floras demonstrate closest correlation to the latest Campanian *Stephanopyxis simonseni* Zone of the recently revised Canadian Arctic diatom zonation[17]. Diatom analysis of core Fl-437 indicates a similar late Campanian age[18]. However, because of conflicting palynological evidence and the lack of any comparable well preserved diatomaceous sequences of early Maastrichtian age dated by other fossil groups, an early Maastrichtian age cannot be ruled out (see Supplementary Information). The core surfaces of both CESAR-6 and Fl-437 displayed macroscopic colour lamination (Fig. 2a), on a millimetre to centimetre scale, for which two strongly conflicting interpretations were proposed. A seasonal alternation of diatom vegetative cells and diatom resting spores was proposed for the Fl-437 core on the basis of sampling from macroscopically visible laminations[2, 18], while analysis of the CESAR-6 core found no differences in diatom content associated with the macroscopic lamination, but attributed the lamination to variations in iron content related to hydrothermal activity[11, 12]. To resolve these competing hypotheses we examined samples using electron microscope techniques (see Methods). Analysis, at a spatial resolution that is only possible using back-scattered electron imagery (BSEI) of resin-embedded sediment, reveals that both cores comprise a regular alternation of laminae composed of two distinctly different diatom assemblages (Fig. 2c,d) that are an order of magnitude thinner than those macroscopically visible. Super-imposed on these laminae of differing diatom composition are changes in the concentration of fine Fe-rich coatings that define the mm to cm-scale macroscopically observed lamination or colour banding[12] (Fig. S-2). Thus, elements of both prior interpretations appear correct. The preservation of undisturbed laminae is consistent with the presence of anoxic bottom waters as would be expected in a basin with strongly stratified waters, analogous to the modern Black Sea, with excess of precipitation over evaporation and only shallow water connections to the world ocean through the Turgay and Fram Straits and

increasingly restricted Western Interior Seaway (Fig. 1)[19]. BSEI analysis of the composition and sequence of the laminae provides new insights into late Cretaceous polar oceanography and climate.

We undertook BSEI analysis of a continuous 58 cm interval from the laminated unit in CESAR-6 (core interval 167.5 – 225.5 cm – see Supplementary Information) complemented by examination of some discrete 2cm long samples from core Fl-437. To verify the integrity of the CESAR-6 section, detailed diatom assemblage counts using optical microscopy were undertaken at 10 cm intervals and these indicate no biostratigraphic change in the diatom flora over the continuously studied interval. More than 3,600 individual laminae of different composition were identified throughout the CESAR-6 interval. We found no evidence for erosional contacts involving truncation of laminae or for current reworking such as ripple cross lamination or lag deposits. From our extensive experience of hemipelagic and pelagic sediments the observed fabrics likely represent an undisturbed record of successive water column flux events.

The diatom laminae within both cores comprise alternations of resting spores with vegetative cells (Fig. 2). The resting spores occur as near monospecific laminae of a small hyaline resting spore resembling modern *Chaetoceros* spp. (Fig. 2d); distinct laminae of this *Chaetoceros*-type resting spore mixed with *Hemiaulus tumidicornis* resting spores and others with less common *Skeletonema subantarctica*. In the modern ocean, diatom resting spore flux is characteristic of the spring bloom in temperate and high latitudes and is normally related to the depletion of nutrients towards the end of the bloom[20]. *Skeletonema* spp. are also a common component of flux from the spring bloom in areas of good opal preservation[14]. The characteristic spring flux of resting spores is also typical of Neogene to recent laminated sediments in which the genus *Chaetoceros* is predominant[14]. In the Cretaceous Arctic Ocean

(as today) there would have been a rapid transition over about one month from complete darkness to continual daylight and without permanent ice cover this would have led to the initiation of the spring bloom and to the development of a strong seasonal thermocline (Fig.3a).

The laminae of diatom vegetative cells that succeed the spring bloom resting spores reflect a different origin. These laminae are dominated by *Hemiaulus* spp. (mainly *H. antiquus* and *H. gleseri* with subordinate *H. danicus* and *H. elegans*) together with *Trochosiropsis polychaeta*, *Anaulus sibiricus* and *Rhizosolenia* spp. all of which may form near-monospecific (or with *Hemiaulus*, near-monogeneric) laminae (Fig. 2c). Recent observations within stratified open-ocean settings such as the North Pacific Subtropical Gyre (NPSG), have identified major blooms of *Hemiaulus hauckii* in association with the nitrogen-fixing, intracellular cyanobacterial symbiont, *Richelia intracellularis*, some of which produce significant export[3]. The Pleistocene and Pliocene organic carbon-rich, Mediterranean sapropels also contain *Hemiaulus hauckii* as a lamina-forming component[4] together with evidence for N_2-fixation[21]. The Cretaceous laminae also contain rhizosolenid diatoms (Fig. 2c) which are often associated with *Hemiaulus* in the modern ocean and in the Mediterranean sapropels and not only may maintain symbiosis with *R. intracellularis* but may also obtain nitrogen through vertical migration to the nutricline[22]. Rhizosolenid diatoms may also thrive at low light levels in deep chlorophyll maxima[14]. Thus, the diatom vegetative cell laminae of the Arctic Cretaceous are consistent with production within stratified waters (Fig. 3b). By analogy with the blooms of the NPSG, nutrients may have been provided by episodic storm-induced eddies[3]. Such blooms might also have been driven by N_2-fixing intracellular symbionts since Si but not N would have been provided by riverine input and/or through vertical migration of the diatoms to tap deep nutrient sources. Strong seasonal stratification

would, indeed, have been expected in the polar summer. Furthermore, Campanian reconstructions from Arctic Canadian Islands evidence significant river run-off to the Arctic Ocean[23] and this freshwater influx would have acted to enhance stratification as well as introducing nutrients. Subsequently, with breakdown of the seasonal thermocline in the rapid transition to the polar night, the diatoms adapted to the stratified conditions would have been rapidly sedimented in a "fall dump"[14] (Fig. 3). Pulses of sedimentation may also have occurred during the summer in response to post-bloom nutrient limitation as has been proposed for some *Hemiaulus hauckii* blooms in the NPSG[24]. In view of the strong seasonal affinity of the two lamina types (Figs. 2, 3) there is a robust case for the combined lamina pair to represent an annual sediment couplet.

The absence of any fragmentation of the diatoms testifies to a rapid post-bloom flux to the sediments occurring before zooplankton populations could respond, possibly complemented by the accumulation of diatom aggregates in "grazer-proof" concentrations in deep chlorophyll maxima prior to flux (Fig. 3). This is in stark contrast to Campanian coastal and shelf sediments from the Canadian Arctic Islands to the south in which there is much fragmented diatom material[23]. The absence of the near-shore, benthic diatom *Paralia* in both the CESAR-6 and Fl-437 cores (present in the Campanian shelf sediments to the south[23]) further indicates a pelagic basinal environment.

In contrast to the modern ocean where the genus *Hemiaulus* is represented by only 4 species, it was one of the dominant genera of the late Cretaceous with over 40 species[25] and may have been better adapted to the less mixed and more stratified seas of the Mesozoic. Intriguingly, biomarker evidence is emerging of cyanobacterial contributions to Cretaceous black shales[26]. It may be that these were produced by cyanobacterial diatom symbionts analogous to *R. intracellularis*, a known symbiont of 3 of the 4 extant *Hemiaulus* species.

Together with complementary biomarker indicators of rhizosolenid diatoms in the late Cretaceous[9], these lines of evidence suggest that diatom algae may already have been key players in the marine biological carbon pump by late Cretaceous times.

An upwelling origin was originally suggested for the diatomaceous sediments of the Alpha Ridge[2], but it is clear from our results that much of the production and export was from highly stratified waters with an initial spring bloom episode and subsequent production in the stratified summer surface layer. The diatom sediment concentrations we measured in the Fl-437 and CESAR-6 cores range between 2 $x10^9$ to $8x10^9$ valves per gram dry sediment, and represent exceptional abundances equalling modern values for the most productive areas of the Southern Ocean. This Cretaceous production, dominated by diatoms adapted to stratified conditions of the polar summer may also be a pointer to future trends in the modern ocean. With increasing CO_2 levels and global warming giving rise to increased ocean stratification[5] this style of production may become of increasing importance.

Our evidence for seasonal diatom production and flux testify to an ice free summer, but the presence of enigmatic lithogenic material suggests the intermittent presence of winter sea ice. Elongate lenses, some isolated grains and very occasional thin laminae of poorly sorted clastic sediment, typically of clay through silt up to fine sand grade occur within about 30% of the annual lamina couplets (Fig. 4). The absence of sorting or any other evidence of density current activity suggests a rafting origin (see Supplementary Information). The lack of material coarser than fine sand rules out glacial ice, or sea ice formed from anchor ice flotation but the size spectrum of particles, in particular the cut-off at fine sand grade, is typical of that of turbid ice which is formed in the modern Arctic by sediment entrainment by frazil ice during fall storms[27, 28]. Such early formed ice is unconsolidated and mobile facilitating long range ice rafting[28]. Although a 15°C mean annual sea surface temperature

(SST) for the late Cretaceous Arctic Ocean has been postulated[9], subsequent papers now propose that the TEX86 method yields a summer SST maximum rather than an annual average[29] allowing for the possibility of significantly colder winter temperatures. Our evidence for the presence of sea ice would be consistent with indications of possible frosts from Campanian-Maastrichtian age tree rings from Ellesmere Island[6]; estimates of polar temperatures down to –10°C from late Campanian-Maastrichtian Alaskan vertebrate enamels[7] as well as models of the late Cretaceous ocean that suggest the formation of seasonal sea ice[8].

METHODS SUMMARY

Samples were obtained from the CESAR-6 core using a sediment slab cutter to extract slabs of the still-wet diatom ooze. Sub-samples of the cut slabs were embedded with resin using fluid-displacive embedding techniques. Six 2 cm palaeomagnetic sample cubes of already dried sediment from the Fl-437 core were embedded by direct infiltration of resin. Polished thin sections were prepared and imaged in a scanning electron microscope (SEM) using backscattered electron imagery (BSEI) to resolve lamina composition. The polished thin sections used for BSEI were also imaged with a flatbed scanner at a resolution of 2400 dpi, in order to closely examine the colour laminations previously reported by visual examination of the core and to compare with the results of BSEI analysis. To complement BSEI, counterpart samples of the sectioned material were prepared for topographic SEM imaging to enable microfossil identification. Detailed diatom micropalaeontology was undertaken using conventional quantitative diatom abundance preparation techniques and optical microscopy. The analysis of a series of diatom micropalaeontology samples from the CESAR-6 core was used to assess the biostratigraphic continuity of the laminated interval.

Full Methods and associated references are available in the online version of the paper at www.nature.com/nature.

.

References

1. Graversen, R. G., Mauritsen, T., Tjernstrom, M., Kallen, E. & Svensson, G. Vertical structure of recent Arctic warming. *Nature* **451**, 53-56 (2008).
2. Kitchell, J. A. & Clark, D. L. Late Cretaceous-Paleogene paleogeography and paleocirculation: evidence of north polar upwelling. *Palaeogeogr. Palaeoclimatol. Palaeoecol.* **40**, 135-165 (1982).
3. Dore, J. E., Letelier, R. M., Church, M. J., Lukas, R. & Karl, D. M. Summer phytoplankton blooms in the oligotrophic North Pacific Subtropical Gyre: Historical perspective and recent observations. *Prog. Oceanogr.* **76**, 2-38 (2008).
4. Kemp, A. E. S., Pearce, R. B., Koizumi, I., Pike, J. & Rance, S. J. The role of mat-forming diatoms in the formation of Mediterranean sapropels. *Nature* **398**, 57-61 (1999).
5. Sarmiento, J. L., Hughes, T. M. C., Stouffer, R. J. & Manabe, S. Simulated response of the ocean carbon cycle to anthropogenic climate warming. *Nature* **393**, 245-249 (1998).
6. Falcon-Lang, H. J., MacRae, R. A. & Csank, A. Z. Palaeoecology of late Cretaceous polar vegetation preserved in the Hansen Point volcanics, NW Ellesmere Island, Canada. *Palaeogeogr. Palaeoclimatol. Palaeoecol.* **212**, 45-64 (2004).
7. Amiot, R. et al. Latitudinal temperature gradient during the Cretaceous Upper Campanian - Middle Maastrichtian: δ18O record of continental vertebrates. *Earth Planet. Sci. Lett.* **226**, 255-272 (2004).

8. Otto-Bliesner, B. L., Brady, E. C. & Shields, C. Late Cretaceous ocean: Coupled simulations with the National Center for Atmospheric Research Climate System Model. *J. Geophys. Res.* **107**, 10.1029/2001JD000821 (2002).

9. Jenkyns, H. C., Forster, A., Schouten, S. & Damste, J. S. S. High temperatures in the Late Cretaceous Arctic Ocean. *Nature* **432**, 888-892 (2004).

10. Moran, K. et al. The Cenozoic palaeoenvironment of the Arctic Ocean. *Nature* **441**, 601-605 (2006).

11. Mudie, P. J., Stoffyn-Egli, P. & Van Wagoner, N. A. Geological constraints for tectonic models of the Alpha Ridge. *J. Geodynam.* **6**, 215-236 (1986).

12. Stoffyn-Egli, P. Iron and manganese micro-precipitates within a Cretaceous biosiliceous ooze from the Arctic Ocean: possible hydrothermal source. *Geo-Marine Lett.* **7**, 223-231 (1987).

13. Sarthou, G., Timmermans, K. R., Blain, S. & Treguer, P. Growth physiology and fate of diatoms in the ocean: a review. *J. Sea Res.* **53**, 25-42 (2005).

14. Kemp, A. E. S., Pike, J., Pearce, R. B. & Lange, C. B. The "Fall dump" - a new perspective on the role of a "shade flora" in the annual cycle of diatom production and export flux. *Deep-sea Res. II* **47**, 2129-2154 (2000).

15. Harwood, D. M., Nikolaev, V. A. & Winter, D. M. in Pond Scum to Carbon Sink: Geological and Environmental Applications of the Diatoms (ed. Starratt, S.) 33-59 (Paleontological Society, 2007).

16. Wagner, T., Damste, J. S. S., Hofmann, P. & Beckmann, B. Euxinia and primary production in Late Cretaceous eastern equatorial Atlantic surface waters fostered orbitally driven formation of marine black shales. *Paleoceanography* **19**, DOI: 10.1029/2003PA000898 (2004).

17. Tapia, P. M. & Harwood, D. M. Upper Cretaceous diatom biostratigraphy of the Arctic archipelago and northern continental margin, Canada. *Micropaleontol*. **48**, 303-342 (2002).

18. Dell'Agnese, D. J. & Clark, D. L. Siliceous microfossils from the warm Late Cretaceous and Early Cenozoic Arctic Ocean. *J. Paleontol*. **68**, 31-47 (1994).

19. Hay, W. W. et al. in *Evolution of the Cretaceous Ocean-Climate System* (eds. Barrera, E. & Johnson, C. C.) 1-47 (Geological Society of America Special Paper 332, Boulder, CO, 1999).

20. McQuoid, M. R. & Hobson, L. A. Importance of Resting Stages in Diatom Seasonal Succession. *J. Phycol*. **31**, 44-50 (1995).

21. Sachs, J. P. & Repeta, D. J. Oligotrophy and nitrogen fixation during eastern Mediterranean sapropel events. *Science* **286**, 2485-2488 (1999).

22. Singler, H. R. & Villareal, T. A. Nitrogen inputs into the euphotic zone by vertically migrating Rhizosolenia mats. *J. Plank. Res*. **27**, 545-556 (2005).

23. Chin, K. et al. Life in a temperate Polar sea: a unique taphonomic window on the structure of a Late Cretaceous Arctic marine ecosystem. *Proc. Roy. Soc. B-Biol. Sci*. **275**, 2675-2685 (2008).

24. Scharek, R., Tupas, L. M. & Karl, D. M. Diatom fluxes to the deep sea in the oligotrophic North Pacific gyre at Station ALOHA. *Mar. Ecol. Prog. Ser*. **182**, 55-67 (1999).

25. Harwood, D. M. & Nikolaev, V. A. in *Siliceous Microfossils* (ed. Blome, C. D., et al (convenors)) 81-106, pls 1-4 (Paleontological Society, 1995).

26. Kuypers, M. M. M., van Breugel, Y., Schouten, S., Erba, E. & Damste, J. S. S. N-2-fixing cyanobacteria supplied nutrient N for Cretaceous oceanic anoxic events. *Geology* **32**, 853-856 (2004).

27. Kempema, E. W., Reimnitz, E. & Barnes, P. W. Sea ice sediment entrainment and rafting in the Arctic. *J. Sedim. Petrol.* **59**, 308-317 (1989).

28. Smedsrud, L. H. Frazil-ice entrainment of sediment: large-tank laboratory experiments. *J. Glaciol.* **47**, 461-471 (2001).

29. Sluijs, A. et al. Subtropical Arctic ocean temperatures during the Palaeocene/Eocene thermal maximum. *Nature* **441**, 610-613 (2006).

Supplemetary Information is linked to the online version of the paper at www.nature.com/nature.

Acknowledgements The research was supported by the award of a NERC Research Studentship (A.D.) and a NERC Research Grant (A.E.S.K. and J. P.). We are grateful to P. Mudie for facilitating sampling of the CESAR-6 core and to D. Clark for providing samples from core FL-437. R. Pearce is acknowledged for assistance with electron microscopy and K. Davis for expertise in drafting. We thank P. Wilson and H. Pälike for comments on the manuscript.

Author Contributions Preliminary SEM and diatom studies of the material were undertaken by J.P. and A.E.S.K. Detailed SEM lamina studies and diatom analysis were performed by

A.D. during PhD studies supervised by A.E.S.K. and J.P. All authors contributed to interpretation. The manuscript was written by A.E.S.K. and incorporates comments from all others.

Author Information Reprints and permissions information is available at www.nature.com/reprints. Correspondence and requests for materials should be addressed to A.E.S.K. (aesk@noc.soton.ac.uk).

Figure Captions

Figure 1. Location of the Alpha Ridge cores. Main Figure: Late Cretaceous palaeogeography of the Arctic region showing location of the Alpha Ridge and other palaeoclimate sites referred to in the text; E – Ellesmere Island[6] and Alaska location[7]. Inset shows modern geography and location of the Alpha Ridge cores: 6 – CESAR-6; 437 – Fl-437; 533 – Fl-533. L.R. – Lomonosov Ridge; M.B. – Makarov Basin. Adapted from the Turonian reconstruction of ref. 9.

Figure 2. Composition of the laminated CESAR-6 core. **a**, Core surface showing the macroscopic colour banding and lamination. Dark blebs are manganese-rich patches[12]. Colour core photo courtesy of P. Mudie. **b**, Back Scattered Electron Image (BSEI) of resin-embedded sediment showing darker, higher porosity, diatom vegetative cell laminae, in which the cross sections of diatoms are discernable, interbedded with paler, lower porosity layers composed primarily of diatom resting spores. **c** and **d**: Representative topographic SEM images of **c**, diatom vegetative cells, mainly *Hemiaulus* spp. but including some rhizosolenid diatoms (marked R); **d**, *Chaetoceros* –type diatom resting spores.

Figure 3. Seasonal cycle of production and flux in the late Cretaceous Arctic Ocean. **a**, Spring bloom. After winter mixing has introduced nutrients to the surface, when light returns and at onset of stratification, the spring bloom occurs. When nutrients are consumed, diatom resting spores form and settle rapidly. **b**, Scenarios for summer production (from left to right): accumulation in a DCM aided by the ability to grow in low light conditions; symbiosis with nitrogen-fixing cyanobacteria providing nitrate for growth; storm-generated

eddies causing doming of isopycnals introducing nutrients to the photic zone. **c**. autumn flux (the fall dump) when stratification breaks down.

Figure 4. Evidence for ice rafting. Thin laminae of poorly sorted terrigenous sediment occurring dominantly within the spring diatom bloom layer. **a**, General view of lamina; **b**, detail of sand-sized grain in **a**; **c**, lamina containing silt and sand sized grains within clay.

Figure 1

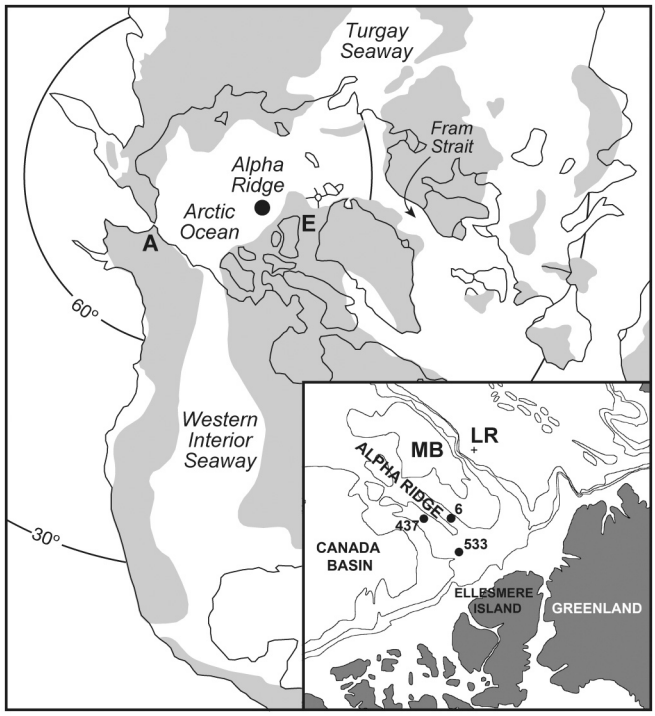
Turgay
Seaway
Fram
Strait
Alpha
Ridge
Arctic
Ocean
E
A
60°
Western
Interior
Seaway
30°
MB
LR
ALPHA RIDGE
6
437
533
CANADA
BASIN
ELLESMERE
ISLAND
GREENLAND

Figure 2

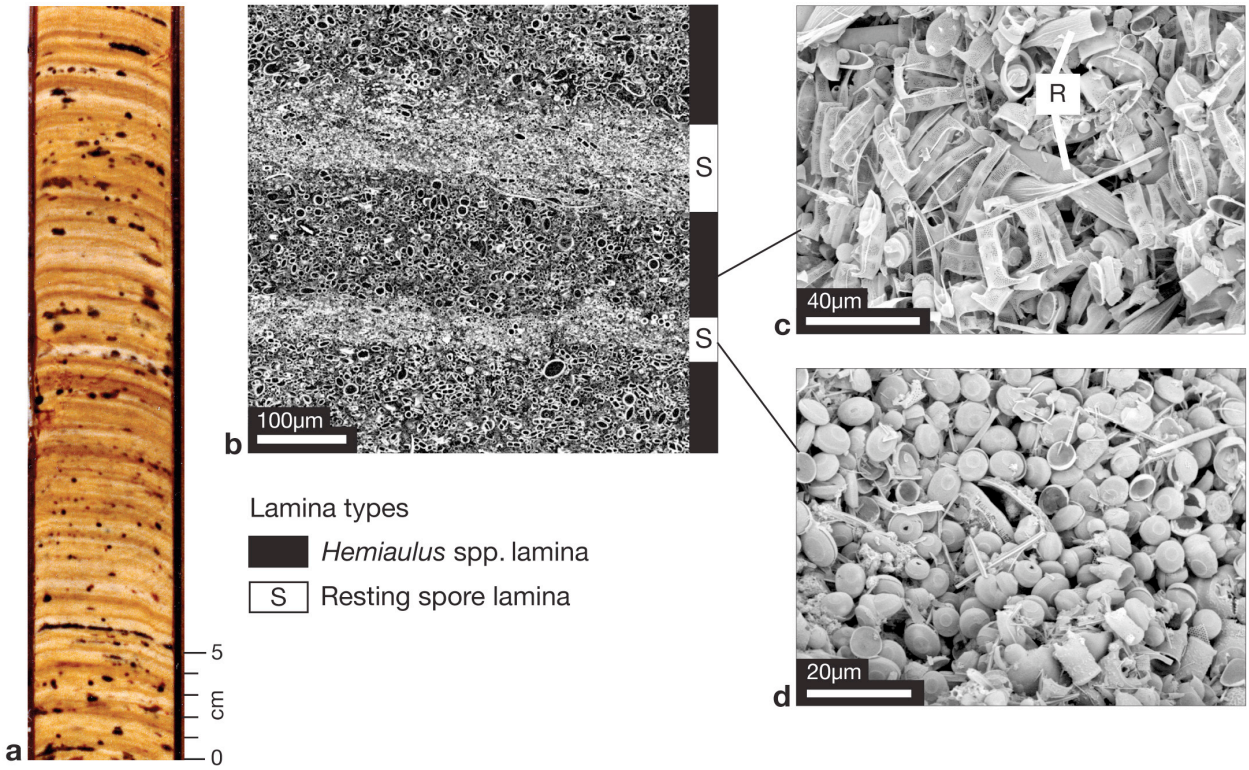
a
5
cm
0
b
100µm
S
S
Lamina types
Hemiaulus spp. lamina
S Resting spore lamina
c
R
40µm
d
20µm

Figure 3

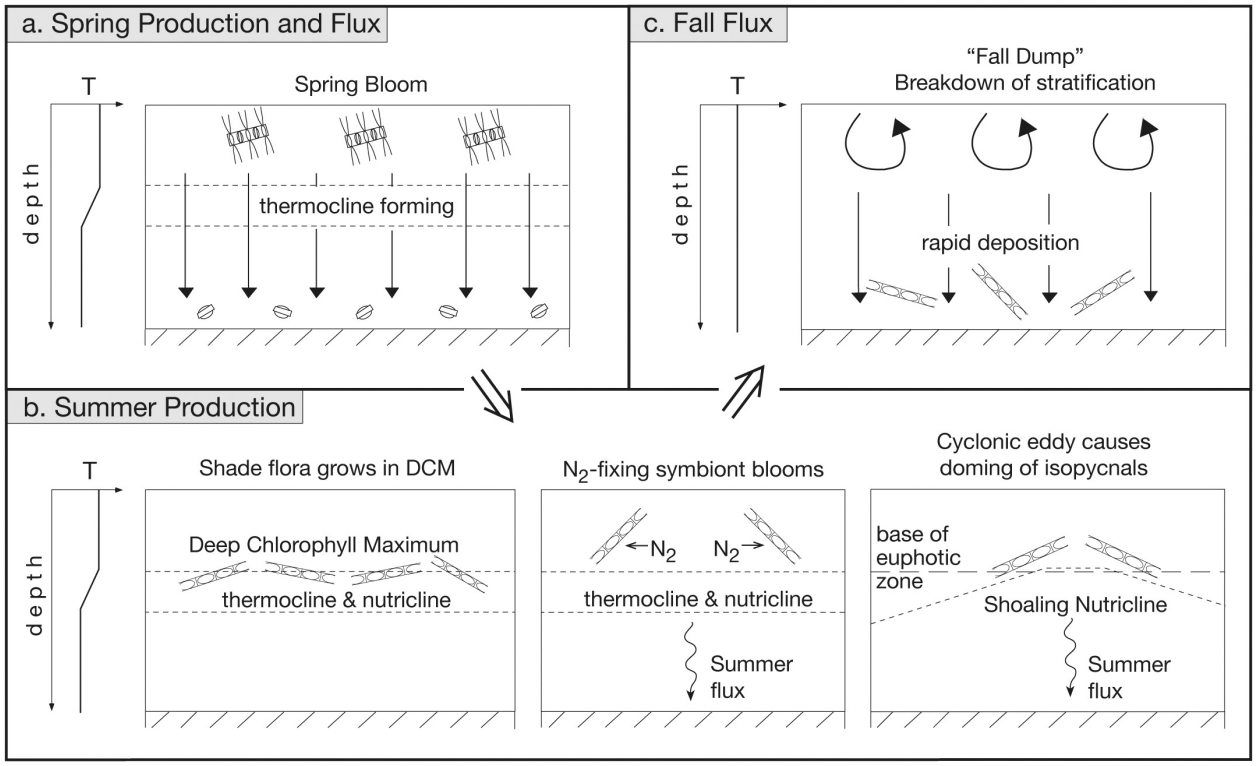
a. Spring Production and Flux
T
depth
Spring Bloom
thermocline forming
c. Fall Flux
T
depth
"Fall Dump"
Breakdown of stratification
rapid deposition
b. Summer Production
T
depth
Shade flora grows in DCM
Deep Chlorophyll Maximum
thermocline & nutricline
N2-fixing symbiont blooms
←N2
N2→
thermocline & nutricline
Summer
flux
Cyclonic eddy causes
doming of isopycnals
base of
euphotic
zone
Shoaling Nutricline
Summer
flux

Figure 4

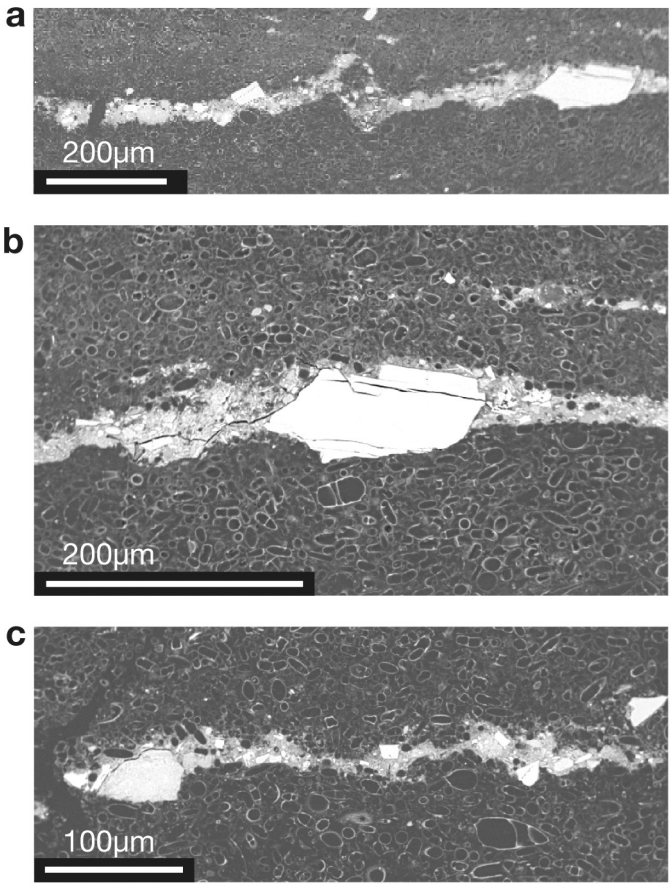

METHODS

Sampling and sample preparation. Samples were obtained from the CESAR-6 core using a sediment slab cutter and sampling protocols following standard procedures[30]. Sub-samples of these were embedded in epoxy resin using fluid-displacive techniques (CESAR-6) [30]. Thin sections of embedded sediment were cut with boundaries oblique to the lamination to ensure continuity between thin sections which were then polished and carbon coated. Six discrete samples of sediment from core Fl-437 were provided in 2cm palaeomagnetic plastic sample cubes. These samples that were already dried were embedded by direct infiltration of low viscosity epoxy resin.

Scanning Electron Microscope methods. Overlapping polished thin-sections were made for the CESAR-6 interval spanning 138 – 305 cm and analysed using a high vacuum LEO 1450VP SEM. Low resolution (66×) BSEI photo-mosaic base maps were produced for each polished thin section by taking 10% overlapping images. Higher resolution (750× and 1000×) photo-mosaics were then produced for more detailed analysis of the interval 167.5 – 222.5 cm. Measurements of individual lamina thickness were made from the high resolution photo-mosaics using the methods of Francus[31]. This method involves the use of the Adobe Photoshop program to mark the boundaries between individual laminae on a digitised photo-mosaic of the polished section. The resultant 'path' is then exported to Microsoft Excel, where a macro converts the measurements into actual thickness using the known quantities of the number of pixels per centimetre on the image (obtained from Photoshop) and the size of individual pixels (obtained from the SEM).

To help better constrain the species make-up of individual laminae, the off-cut portions of individual polished thin sections were kept and used to make topographic stubs. Laminae of

interest were carefully fractured and fixed onto SEM stubs using carbon based wax for SEM analysis. As a complement to the topographic stubs, peel slides were taken of the raw material using double sided carbon tape. These provided topographic images of the diatoms *in situ* with very little disturbance to the sedimentary microfabric. As microfabrics were analysed primarily from the cross-sectional images obtained from the polished thin sections, the peels greatly facilitated the task of diatom identification within individual laminae. Suitable sized pieces of tape were cut to fit onto standard SEM glass slides. The tape was placed on the surface of the sediment block and gently pressed to ensure contact was made along the entire length of the tape. The tape was then carefully peeled off and affixed onto a glass slide. Two peels were made for each section studied and affixed to the same glass slide. The slides were subsequently coated in gold in preparation for use with the SEM. The polished thin sections used for BSEI were also imaged with a flatbed scanner at a resolution of 2400 dpi, in order to closely examine the colour laminations previously reported by visual examination of the core and to compare with the results of BSEI analysis.

Diatom Micropalaeontology. Diatom strew slides were prepared from 19 samples of CESAR-6 Unit 4 (see Supplementary Information). To ensure several laminae were included in all slides, samples were comprised of material homogenised from 1 cm of the core. Samples were taken at intervals of 10 cm, from 138 cm – 298 cm, with additional samples taken at 134 cm and 305 cm. Samples were digested and prepared using an adaptation of the method of Scherer[32] (Claire S. Allen, personal communication, 2004). This method was found to produce an even spread of diatomaceous material over whole the coverslip, without bunching of frustules. Quantitative analyses were performed at 500×, with identifications checked at ×1000. Counts were made along several traverses of the cover slips.

Quantitative diatom abundances, or concentrations, were also calculated for two samples from the CESAR-6 core (210.5 – 210.8 cm, 211.8 – 212.1 cm), and one from the Fl-437 core (sample Fl-437-13-2), prepared using the digestion and random settling method of Bodén[33]. Diatoms were counted using 1000× magnification and concentrations were calculated using the following formula: Concentration (valves/g) = (WD × AC × ND)/(WS × AV × NV × VS) where WD is the mass of sample solution in grammes, AC is the area of the settling container in mm^2, ND is the number of diatom valves counted, WS is the dry weight of the initial sample in grammes, AV is the area of the field of view (or transect) in mm^2, NV is the number of fields of view (or transects) and VS is the mass of the sub-sample solution in grammes[33].

30. Kemp, A. E. S., Dean, J., Pearce, R. B. & Pike, J. *in Tracking Environmental Change Using Lake Sediments. Volume 2: Physical and Geochemical Methods* (eds Last, W. M. & Smol, J. P.) 7-22 (Kluwer, 2001).

31. Francus, P., Keimig, F. & Besonen, M. An algorithm to aid varve counting and measurement from thin-sections. *J. Paleolimnol.* **28**, 283-286 (2002).

32. Scherer, R. P. A new method for the determination of absolute abundance of diatoms and other silt-sized sedimentary particles. *J. Paleolimnol.* **12**, 171-179 (1995).

33. Bodén, P. Reproducibility in the random settling method for quantitative diatom analysis. *Micropalaeontology* **37**, 313 (1991).

Supplementary Information

Late Cretaceous seasonal ocean variability from the Arctic.

Andrew Davies[1‡], Alan E. S. Kemp[1]*, Jennifer Pike[2]

[1] National Oceanography Centre Southampton, School of Ocean and Earth Science, University of Southampton, Southampton, SO14 3ZH, UK.

[2] School of Earth and Ocean Sciences, Cardiff University, Main Building, Park Place, Cardiff, CF10 3YE, UK.

*To whom correspondence should be addressed, E-mail: aesk@noc.soton.ac.uk

‡ Present address: Neftex Petroleum Consultants Ltd, 97 Milton Park, Abingdon, OX14 4RY, UK.

Supplementary Information

Diatom micropalaeontology and biostratigraphy

Diatom strew slides were prepared from 19 samples of CESAR-6, Unit 4 (Fig. S1 and see methods). A total flora list is given in Table S1 and the detailed counts are given in Tables S2 and S3. In an earlier study two samples from the CESAR-6 core and one sample from core Fl-437 were analysed and diatom concentrations in valves/ gramme were calculated (see methods) (Table S4). In keeping with Barron's earlier diatom micropalaeontological study [S1] we find no evidence for evolutionary biostratigraphic change within Unit 4 of the CESAR-6 core. Barron [S1] assigned a Late Campanian age to the CESAR-6 diatom ooze based on Strelnikova's biostratigraphic divisions of the diatom assemblages of the Ural Mountains, Russia [S2, S3]. At the time of Barron's initial study only one other diatom biostratigraphical scheme existed for the Late Cretaceous; that of the southern high-latitude Campbell Plateau DSDP Site 275 cores (50°26'S, 176°19'E). Hajós & Stradner [S4] tabulated 124 diatom taxa from the two upper Campanian cores recovered from this site. Although many of the key taxa used in the zonation scheme do not occur in the CESAR-6, Barron [S1] found a moderate correlation between the CESAR-6 assemblages and that of DSDP Site 275, substantiated by the current study. From the analysis of four Canadian Arctic sections spanning the Upper Cenomanian – latest Campanian, Tapia and Harwood [S5], tabulated 203 diatom taxa from which they proposed four Upper Cretaceous diatom biostratigraphical zones. Comparisons with each of these biostratigraphical zones show that, in general, the CESAR-6 flora bears a close similarity with those of the early Late Campanian *Trinacria indefinita* and late Late Campanian *Stephanopyxis simonseni* zones, although both *T. indefinita* and *S. simonseni* are absent from the CESAR-6 core. Numerous CESAR-6 taxa are present in both zones (e.g. *A. tenuis, G. odontella, H. altus, H. kittonii, P. cretacea, S. steinyi,*

S. turris, T. wittiana, T. planum, *T. acutangulum* and *T. polychaeta*). However, *T. polychaeta* (which is abundant in the CESAR-6) is rare in the *Trinacria indefinita* zone and is more characteristic of the *Stephanopyxis simonseni* zone. *H. tumidicornis* (also abundant in the CESAR-6) is also only found in the *S. simonseni* zone, and *A. sibiricus* is more abundant in this zone, indicating that the CESAR-6 diatoms have closest affinity with the Late Campanian *Stephanopyxis simonseni* Zone. There may be environmental factors that explain the absence of *S. simonseni* that relate to the uniquely distal (remote from land) pelagic setting of the CESAR-6 and Fl-437 cores compared to other late Cretaceous diatomaceous sequences. The near-shore benthic diatom *Paralia* is not present in CESAR-6 or Fl-437 and *Stephanopyxis* species are rare. This is in contrast to the other well preserved late Cretaceous diatomaceous sequences that contain diverse and common *Stephanopyxis* spp. and all of which are marginal or shelf facies (published accounts of Seymour Island –Maastrichtian [S6]; Canadian Arctic Islands – Campanian [S5]; West Siberia – Campanian to ?Maastrichtian [S2]; Marca Shale – late Maastrichtian [S7, S8, Davies, A., Ph.D. Thesis, University of Southampton, 2006]. On this basis, it is likely that *Stephanopyxis* was predominantly a marginal or shelf genus at this time and this may explain the absence of *Stephanopyxis simonseni* on the Alpha Ridge. There is no published account of an early Maastrichtian diatomaceous sequence dated by other fossil groups so that an early Maastrichtian age may be possible. However, Tapia and Harwood [S5] make reference to unpublished data of Nikolaev and Harwood from the Kerguelen Plateau (ODP Leg 120, Site 748) of an early Maastrichtian occurrence of *Azpeitia morenoensis*. *A. morenoensis* is not present in CESAR-6 or FL-437, so that unless environmental factors are involved, an early Maastrichtian age appears unlikely. The considerable differences with the flora of the late Maastrichtian Marca Shale rule out a late Maastrichtian age [S1; Davies, A., Ph.D. Thesis, University of Southampton, 2006].

Biostratigraphic data for the CESAR-6 and Fl-437 cores have also been obtained from silicoflagelates and palynological studies. Although Bukry [S9] assigned a Maastrichtian age for CESAR-6 he noted that: "The distinctive species array at Alpha Ridge is believed to result from progressive ecological restriction, probably during the middle or late Maastrichtian. A correlation earlier in the Cretaceous cannot be ruled out, because there is a lack of high-latitude reference localities which would permit distinction of ecological and evolutionary changes." Mudie [S10] recorded Maastrichtian dinoflagellates from the diatomaceous interval of CESAR-6 (Unit 4; see Figure S-1) but noted that some stratigraphic guide taxa "may not be conspecific with Arctic Islands and North Atlantic taxa". In a reappraisal of Mudie's data, Firth and Clark [S11] endorse a Maastrichtian age for CESAR-6 Unit 4 on the basis of a key dinoflagellate species and pollen dated as Maastrichtian from a single Arctic Island sequence. In summary, while diatom biostratigraphy has closest affinities with the late Campanian, the conflicting palynology opens the possibility of an early Maastrichtian age.

Macroscopic lamination in the cores

The distinction between the macroscopic mm to cm scale, yellow to pale grey lamination visible in the core surfaces (Fig. 2) and the 100 micron scale lamination identified in BSEI is shown in Figure S2 where a flat bed scan of a resin – embedded counterpart is shown next to a back scattered electron image (BSEI) of a polished thin section of an off-cut of the same slab. Unit 4 of the CESAR-6 core contains a well-preserved, pervasive laminated succession of alternating diatomaceous vegetative cells and smaller, more heavily silicified resting stages readily identified in BSEI (Fig. 2). These diatom vegetative cell/ resting spore laminae are an order of magnitude thinner than the colour laminations visible on the core surface and described by earlier workers (Fig. S2). The colour laminations are independent of and

overprint the compositional laminae (i.e. the diatom vegetative/resting spore laminae). The yellow macroscopic colour laminae are enriched in iron that was identified as Fe-rich flocs coating diatoms (S13) and may be marked by a brighter BSEI (Fig. S2) and also identified by energy dispersive X-ray microanalysis. Analysis of the high resolution flatbed scans of the polished thin sections used in this study (Fig. S2) reveal that the yellow coloured laminations range in thickness from 265-4636 μm (mean 980 μm) whilst the pale grey coloured laminations range from 187-6536 μm (mean 769 μm). Consequently, the mean thickness of a yellow/ pale grey coloured laminae couplet is 1749 μm. In contrast, the mean thickness (measured using BSEI) of vegetative cell laminae, resting spore laminae and the total couplet is 123.8 μm, 125.5 μm and 250.1 μm respectively. Using these figures, each yellow-pale lamina couplet therefore contains on average 7 vegetative cell/resting spore lamina couplets. Any study into compositional differences using sampling from the core from the macroscopic colour laminations would be unable to detect the alternating vegetative cell/resting spore laminations through too coarse a sampling resolution.

Lithogenic sediment in the laminae

The lithogenic material within the CESAR-6 core that occurs in about 30% of annual couplets is composed of clay and silt grade with more minor very fine sand and fine sand grade particles. Mineralogical analysis of the silt and sand grade material indicates the dominance of quartz and feldspar with a minor component of volcanic glass. The critical features of the lithogenic component in the Alpha Ridge cores that require explanation are the lack of sorting in the lithogenic lenses, the dominance of clay and silt but the presence of up to (but not coarser than) the fine sand size fraction. The poor sorting of the material combined with the lack of any evidence of current activity in the cores (e.g. scour; grading, cross lamination)

suggests a rafting origin. Although organic rafting of marine sediment may be locally important, the high frequency of the Alpha Ridge rafting events together with the lack of material coarser than fine sand makes this an unlikely agent (S14). If there was a component of glacial ice supply one would expect to see particles much coarser than just fine sand grade (medium and coarse sand, granules and larger drop stones) but there is no evidence of any such clasts in either the CESAR-6 or the Fl-437 core. Similarly, sea ice formed from anchor ice flotation or by seabed freezing in shallow water with subsequent flotation would also be expected to have a much coarser size range (S15). However, the formation and flotation of frazil ice in fall storms incorporates fine suspended sediment of mainly clay and silt grade (but including small amounts of fine sand) and this rises to the surface to be incorporated into slush ice, ultimately forming "turbid ice" in the modern Arctic (S15). When such layers initially form, the sea ice is unconsolidated and highly mobile. In the modern Arctic such material may be advected off shelf areas and can deliver material to the deep Arctic Basin (S15).

An origin through frazil ice incorporation also explains the consistent maximum particle size of the Alpha Ridge material. Experimental research demonstrates that that no grains larger than 250 microns become aggregated to frazil ice (S16). This is exactly the cut-off in our Alpha Ridge layers. The grain size distribution of the layers is also consistent with the distinction between sea-ice derived material and hemipelagic sediment as indicated from sediment trap studies (S17).

S1. Barron, J. A. in Initial Geological Report on CESAR-the Canadian Expedition to Study the Alpha Ridge (eds. Jackson, H. R., Mudie, P. J. & Blasco, S. M.) 137-148 (Geological Survey of Canada, Paper 84-22, Report 10, 1985).

S2. Strelnikova, N. I. Late Cretaceous diatoms of western Siberia (Academie Nauk, SSSR, Roy. 8, 1974).

S3. Strelnikova, N. I. in Third symposium on Recent and Fossil Diatoms 311-321 (Nova Hedwigia, Beihefte, Kiel, 1975).

S4. Hajós, M. & Stradner, H. in Initial Reports of the Deep Sea Drilling Project **275**, 913-1009 (Washington D.C., 1975).

S5. Tapia, P. M. & Harwood, D. M. Upper Cretaceous diatom biostratigraphy of the Arctic archipelago and northern continental margin, Canada. *Micropaleontol.* **48**, 303-342 (2002).

S6. Harwood, D. M. Upper Cretaceous and lower Paleocene diatom and silicoflagellate biostratigraphy of Seymour Island, eastern Antarctic Peninsula. *Geol. Soc. Am. Mem.* **169**, 55-129 (1988).

S7. Nikolaev, V. A., Kociolek, J. P., Fourtanier, E., Barron, J. A. & Harwood, D. M. Late Cretaceous diatoms (Bacillariophyceae) from the Marca Shale Member of the Moreno Formation, California. *Occasional Papers of the California Academy of Sciences* **152**, 119 p (2001).

S8. Fonseca, C. in Marine Authigenesis: from global to microbial (eds. Glen, C. R., Prévôt-Lucas, L. & Lucas, J.) 455-480 (SEPM (Society for Sedimentary Geology) Special Publication 66, 2000).

S9. Bukry, P.J. in Initial Geological Report on CESAR-the Canadian Expedition to Study the Alpha Ridge (eds. Jackson, H. R., Mudie, P. J. & Blasco, S. M.) 455-480 (Geological Survey of Canada, Paper 84-22, Report 9, 1985).

S10. Mudie, P.J. in Initial Geological Report on CESAR-the Canadian Expedition to Study the Alpha Ridge (eds. Jackson, H. R., Mudie, P. J. & Blasco, S. M.) 149-174 (Geological Survey of Canada, Paper 84-22, Report 11, 1985).

S11. Firth, J.V & Clark, D.L. An early Maastrichtian organic-walled phytoplankton cyst assemblage from an organic-rich black mud in core Fl-533, Alpha Ridge: evidence for upwelling conditions in the Cretaceous Arctic Ocean *Mar. Micropaleontol.* **34**, 1-27 (1998).

S12. Mudie, P. J. & Blasco, S. M. in *Initial Geological Report on CESAR - the Canadian Expedition to Study the Alpha Ridge, Arctic Ocean* (eds. Jackson, H. R., Mudie, P. J. & Blasco, S. M.) 59-99 (Geological Survey of Canada, Paper 84-22, report 6, 1985).

S13. Stoffyn-Egli, P. Iron and manganese micro-precipitates within a Cretaceous biosiliceous ooze from the Arctic Ocean: possible hydrothermal source. *Geo-Marine Lett.* **7**, 223-231 (1987).

S14. Emery, K.O. in *The Sea* (ed. Hill, M.N.) 776-793 (John Wiley, Volume 3, 1963).

S15. Kempema, E. W., Reimnitz, E. & Barnes, P. W. Sea ice sediment entrainment and rafting in the Arctic. *J. Sedim. Petrol.* **59**, 308-317 (1989).

S16. Smedsrud, L.H. Frazil-ice entrainment of sediment: large-tank laboratory experiments. *J. Glaciol.* 4**7**, 461-471 (2001).

S17. Hebbeln, D. Flux of ice-rafted detritus from sea ice in the Fram Strait. *Deep-Sea Res. II* **47**, 1773-1790 (2000).

Table S1: CESAR-6 diatom flora list. Informal names generated for this study are indicated with an asterisk; those from existing literature are referenced. This includes identifications from electron microscopy in addition to those identified by optical microscopy (Table S3).

Acanthosphaeridium reticulatum	*H*. sp. 3*
Actinoptychus simbirkianus	*H*. sp. 4*
A. tenuis	*H*. sp. 5*
Anaulus sibiricus	*H*. sp. 6*
A. sp 1*	*H*. sp. 7*
Cerataulina cretacea	*H*. sp. G[2]
*Chaetoceros-type Spore '1'**	*H*. spore 1*
Coscinodiscus circumspectus	*H*. spore 3*
C. sibiricus	*Odontotropis cristata*
C. symbolophorus	*Proboscia cretacea*
Gladiopsis pacificus	*Pseudopyxilla americana*
G. speciosa	*P. russica*
Goniothecium odontella	*P*. sp Strelnikova[3]
Helminthopsis wornardti?	*Pterotheca crucifera*
Hemiaulus altus	*P*. of Strelnikova (1974)[4]
H. ambiguus	*Rhizosolenia sp.*
H. antiquus	*Sceptroneis dimorpha*

H. danicus	*S.* sp. B*
H. elegans	*Skeletonema subantarctica*
H. gleseri	*Skeletonemopsis crawfordii*
H. giganteus	*Stellarima steinyi*
H. hostilis	*S.* sp. 2*
H. includens	*Stephanopyxis turris*
H. kittonii	*Thalassiosiropsis wittiana*
H. oonki	*Triceratium indefinitum*
H. polymorphus var. *morianus*	*T. planum*
H. rossicus	*Trinacria acutangulum*
H. tumidicornis	*T. tessela*
H. sp. Barron[1]	*Trochosiropsis polychaeta*
H. sp. 2*	

[1] Barron (1985) (S1) pl. 10.2 fig. 9

[2] Harwood (1988) (S6) fig. 14.6

[3] Strelnikova (1974) (S2) pl. 54, fig. 16

[4] Strelnikova (1974) (S2) pl. 57, fig. 33-34

Table S2: CESAR-6 diatom strew slide counts inclusive of *Chaetoceros*-type spores and chrysophytes.

sample	CESAR-6 depth in core cm	Chrysophytes	*Chaetoceros*-type spores	Other valves	Total
19	134-135	71	26	409	506
1	137.5-138.5	53	73	350	476
2	147.5-148.5	30	96	378	504
3	157.5-158.5	86	20	336	442
4	167.5-168.5	33	39	343	415
5	177.5-178.5	72	51	362	485
6	187.5-188.5	56	54	236	346
7	197.5-198.5	4	102	290	396
8	207.5-208.5	62	84	213	359
9	217.5-218.5	34	74	216	324
10	227.5-228.5	38	81	278	397
11	237.5-238.5	19	128	228	375
12	247.5-248.5	42	100	198	340
13	257.5-258.5	45	82	224	351
14	267.5-268.5	65	52	360	477
15	277.5-278.5	61	61	210	332
16	287.5-288.5	54	42	475	571
17	297.5-298.5	143	8	200	351
18	304-305	106	10	201	317

Table S3: CESAR-6 diatom strew slide counts exclusive of Chaetoceros-type spores and chrysophytes. See Table S2 for sample depth in core. Informal species names are those of this study unless indicated in superscript (below) reference to footnote of Table S1.

	Sample number																		
	19	**1**	**2**	**3**	**4**	**5**	**6**	**7**	**8**	**9**	**10**	**11**	**12**	**13**	**14**	**15**	**16**	**17**	**18**
Anaulus sibiricus	171	85	43	100	51	98	27	34	50	27	50	33	37	53	73	49	81	227	201
Trochosiropsis polychaeta	23	46	42	21	8	27	26	30	35	31	51	32	54	45	37	44	27	4	2
Hemiaulus tumidicornis	117	88	125	250	276	261	131	137	120	160	96	170	133	131	218	183	284	26	41
H. antiquus	20	27	16	38	6	23	24	31	25	29	21	5	18	22	21	6	15		2
H. danicus	5	4	2	4	1	1	3	1	4	6	2	4	3		3		3	7	1
H. gleseri	36	34	17	35	17	44	22	25	25	22	37	19	5	15	17	16	11	17	26
H. elegans	2	4				1	1		2	4	1	3		2			3	1	1
H. oonki	1			1	1	2						1	1			1		14	2
H. sp. Barron[1]	3	8	10	17	5	5	2	22	7	14	3	17	13	13	15	15	9		1
H. G[2]				1															
H. kittoni				1			1												
H. spore 1	52	43	55	61	32	47	52	76	49	71	139	67	132	82	103	111	64	9	9
H. spore 3	17	4	28	15	8	11	17	15	5	11	14	31	28	16	24	28	29	3	1
other *Hemiaulus* spp	1	1				1				1	4					2		1	3
H. hostilis		1		2		1				1						1			
H. giganteus										1							1		
H. rossicus	2					1				1				1	1			5	
H. includens																		2	
Hem sp. 2	2			8		1				2							1		
Hem sp. 3											1								1
Hem sp. 4															1				
Hem sp. 5																1	2	1	
Hem sp. 6	1			1															
Hem sp. 7					1														
Coscinodiscus circumspectus		2	1			1			1								1		
Acanthosphaeridium	2	4	1	3	3	2	5	1	2	8	4	12	6	23	2	10	7	40	8

reticulatum																			
Actinoptychus spp.	2	1	1	1			1	1				1	2		1	1		3	6
Skeletonemopsis crawfordii	1			1		1		1			1	1		1				21	5
Rhizosolenia (thick)	1	8	1	6	4	7	1	4	3	2	2	1	1	3		1	1	7	6
Rhizosolenia (thin)	9	13	3	4	3	4	8	10	8	3	9	3	2	7	8	1	2	11	11
Ceratulina cretacea		7		1		1			1	2		3	1		2	1	3	1	
Pseudopyxilla	15	6	7	20	8	10	3	7	10	10	12	10	7	8	10	7	8	9	3
Skeletonema subantarctica	9	3	2	6	5	3	5	3	6	14	10	12	5	6	5	7	8	7	4
Stephanopyxis spp.								1					2		2				
Trinacria tessela	1					3	1												
Triceratium indefinitum	1	1						1	1									1	
Pennate spp.			1	2		6	4		7	8	1		2	1	3	2	9	1	2
Gladiopsis spp.	1	1	1					1											1
Trinacria acutangulum		2				3		2	1				1		1	1		1	
Pterotheca spp.					2						1		1	1		2			
Pseudopyxilla sp. Strelnikova[3]																		26	53
Stellarima spp.				1	2							1							
Proboscia cretacea		2	3		1	1	5	1	4	6	6	1	2	14	8	4	1	1	3
Goniothecium odontellum				2											2				
Thalassiosiropsis wittiana																			1
Coscinodiscus sibiricus																			1
Anaulus sp. 1				15															
totals	495	395	359	617	434	566	339	404	366	434	465	427	456	444	557	494	570	446	395

Table S4: Quantitative diatom counts from CESAR-6 and Fl-437 undertaken in an earlier pilot study by J. Pike (informal species names are those of Pike).

	JP2B	JP3B	JP4A
	CESAR-6	CESAR-6	Fl-437 (13-2)
	211.8 - 212.1 cm	210.5 - 210.8 cm	
Actinoptychus spp.	2	2	
Anaulus spp.	3		
??*Chaetoceros* sp. 1	3	3	2
Coscinodiscus spp.	7	2	1
Debya/*Aulacodiscus*	1		1
Hemiaulus spp.	159	245	196
Horodiscus sp.?		9	3
Pseudopyxilla spp.	6	11	14
Pterotheca spp.	5	10	3
Rhizosolenia spp.	7	3	1
Sceptroneis spp.	2	4	
Stephanopyxis spp.	5	7	2
Triceratium spp.	1		
Trinacria spp.	1		
Resting spores (airfilled x2)	66	68	102
Resting spore (halves)	306	169	176
Resting spore (long)	6	9	5
Unidentified centrics	3	4	7
Unidentified pennates	1		1
Stellarima fragments	1	1	
Total	585	547	514

WD	49.509	49.608	47.587	mass sample solution, g
AC	5947.071	5947.071	5947.071	area of petri dish, mm^2
ND	585	547	514	no. valves counted
WS	0.089	0.042	0.041	dry weight, g
AR	0.258	1.032	1.462	transect area, mm^2
VS	1	1	1	mass of sub sample solution g
valves/g dry sediment	7501246940	3723172959	2426740684	
	$7.50x10^9$	$3.72x10^9$	$2.42x10^9$	

Notes: Resting spores (airfilled x2): figure is the no. counted multiplied by 2

Stellarima fragments: 1 valve was added where fragments were identified

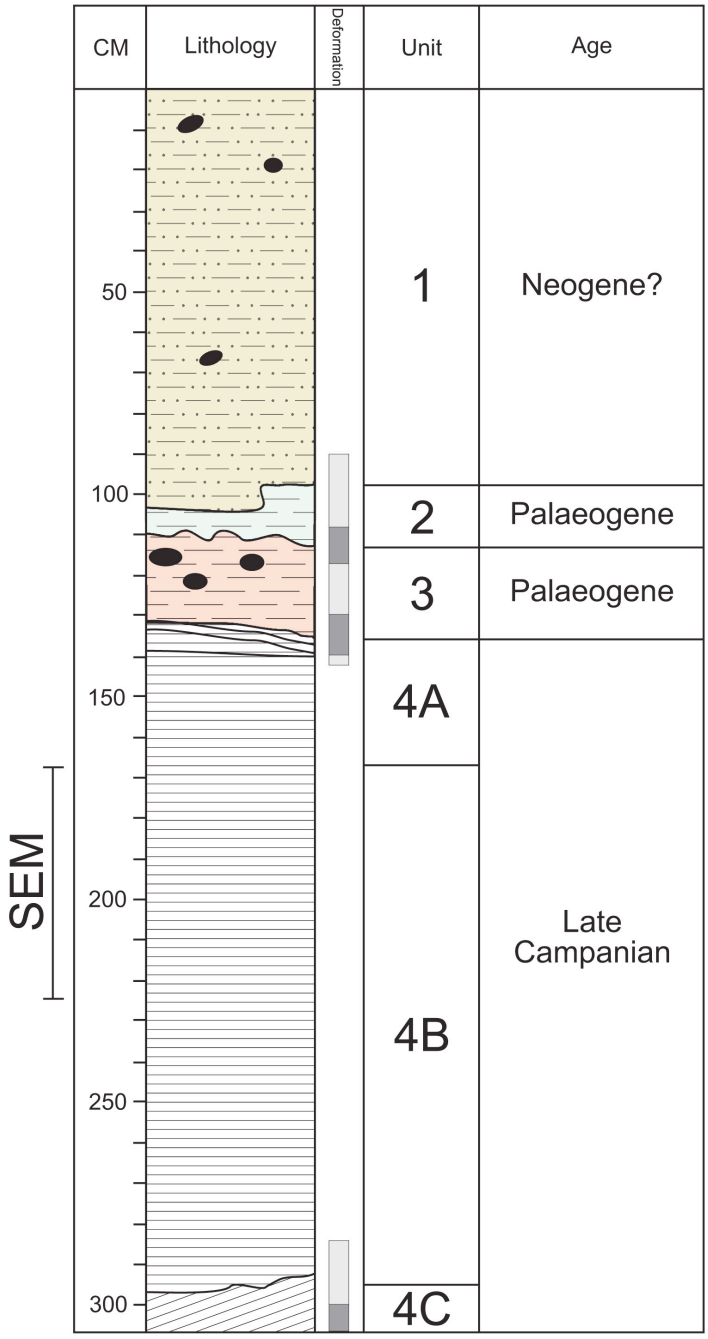

Figure S1. Generalised log of the CESAR-6 core showing main lithological units after Mudie and Blasco (S7). Deformation marks as indicated in original description of Mudie and Blasco (S7). The late Campanian diatom ooze is Unit 4 (see text for discussion of age model). The mark SEM indicates the section where detailed lamina identification and counting was undertaken in the core interval 167.5 – 225.5 cm.

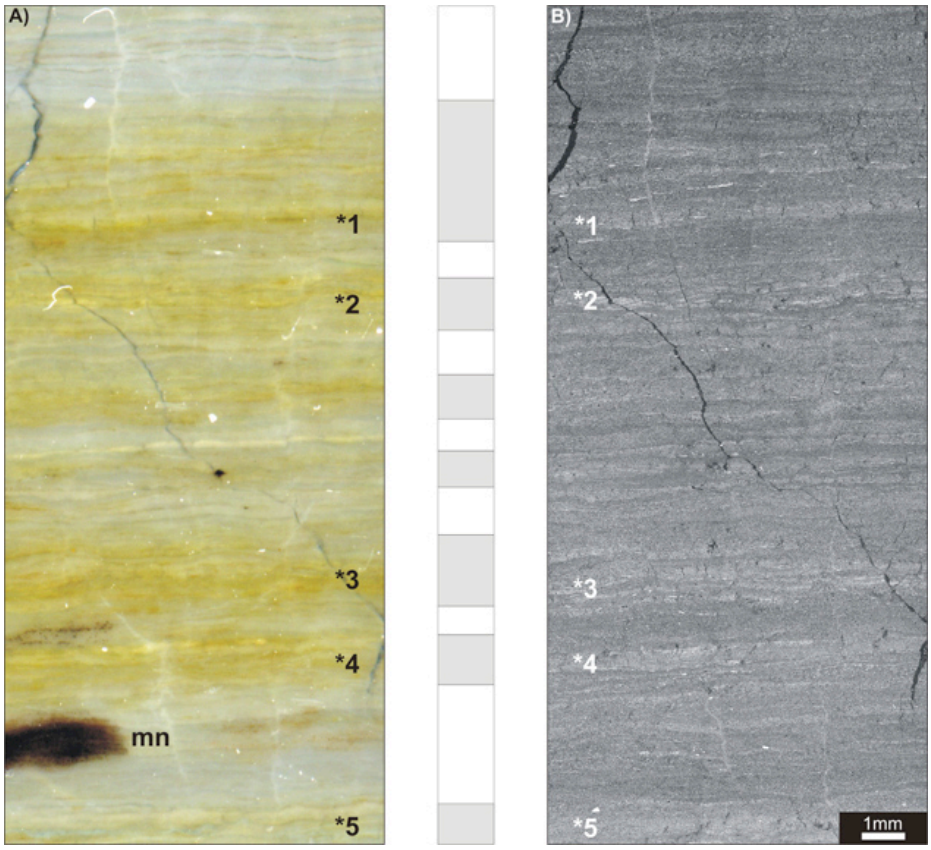

Figure S2 Left: (A) shows a flat bed scan of a resin-embedded block of sediment. This shows the mm to cm scale alternating yellow and pale grey lamination that is clearly visible in the core surfaces and indicated in the log column to the right. The yellow laminae have higher concentrations of iron. Right: (B) Backscattered Electron Image (BSEI). Note the compositional laminations visible pervasively in the BSEI (although the detailed lamina composition is not visible at this scale) and that the colour laminations are not discernable in the BSEI. However, some of the yellowish mm scale laminations (numbered) do have a brighter appearance in BSEI because higher concentrations of Fe result in a higher backscatter coefficient (cf. S13). The variation in Fe content is verified by energy dispersive X-ray microanalysis. Note also the black spot (Mn) is not seen in BSEI.